Biophysical Chemistry 177–178 (2013) 7–13

Contents lists available at SciVerse ScienceDirect

Biophysical Chemistry

journal homepage: http://www.elsevier.com/locate/biophyschem

Light scattering methods for tracking gold nanoparticles aggregation induced by biotin–neutravidin interaction

Ines Delfino *

Biophysics and Nanoscience Centre, Dipartimento di Scienze Ecologiche e Biologiche, Università della Tuscia, Viterbo, Italy

HIGHLIGHTS

- Neutravidin in nM-concentration range was revealed by light scattering methods.
- Biotin coated gold nanoparticles were used as probes.
- Scattering signal changes were related to nanoparticle aggregate characteristics by Mie theory predictions.
- Potentials of light scattering methods for bio-sensing applications were confirmed.

GRAPHICAL ABSTRACT

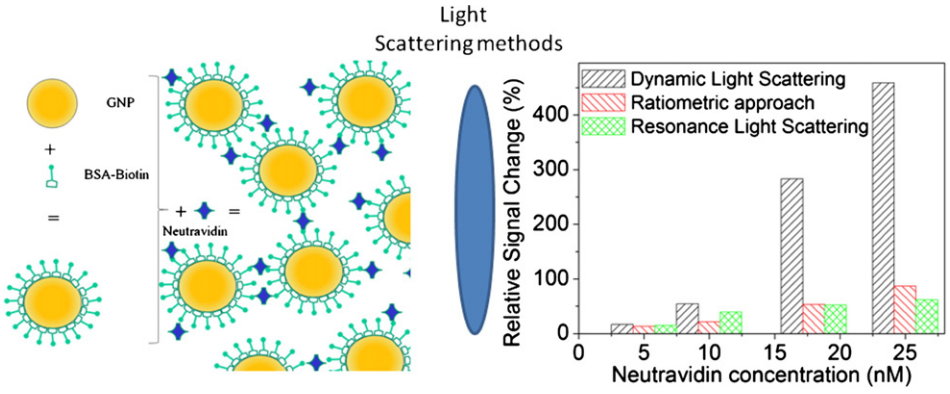

ARTICLE INFO

Article history:
Received 14 January 2013
Received in revised form 4 March 2013
Accepted 4 March 2013
Available online 15 March 2013

Keywords:
Light scattering methods
Neutravidin
Biomolecule-coated gold nanoparticles
Biotin–neutravidin interaction
Optical biosensors

ABSTRACT

Dynamic and Static Light Scattering (DLS and SLS), Resonance Light Scattering (RLS) and angular-ratiometric methods have been used for investigating the aggregation of biotinylated bovine serum albumin gold nanoparticles induced by the interaction of biotin with its partner neutravidin. All the approaches have shown to be sensitive to the presence of neutravidin in solution at nM-concentrations. Changes in scattered light intensity dependence on the scattering angle (studied by SLS) and on the wavelength of the incident light (by RLS) have been observed. Predictions from Mie theory have enabled to connect these changes to the increase in the hydrodynamic size of the aggregates, quantified by DLS. The results here reported confirm the potentials of light scattering approach for realizing methods for analyte quantification and offer a good starting point for evaluating the limits and advantages of each method, which would further widen the use of light scattering approach in biosensing.

1. Introduction

In recent years, gold nanoparticles have been extensively studied and used in various applications because of their unique optical and catalytic properties [1–12]. The optical properties are due to electron oscillations in the metallic particles, induced by the incident light field, giving rise to the so-called plasmon absorption [1–5]. The efficiency of gold nanoparticles (GNPs) to absorb and scatter light is highly

* Biophysics and Nanoscience Centre, Dipartimento di Scienze Ecologiche e Biologiche, Università della Tuscia, I-01100 Viterbo, Italy. Tel.: +39 0761 357026; fax: +39 0761 357027.
E-mail address: delfino@unitus.it.

0301-4622/$ – see front matter © 2013 Elsevier B.V. All rights reserved.
http://dx.doi.org/10.1016/j.bpc.2013.03.001

dependent on the size and the shape of the GNP and on the dielectric properties of the environment [5,13,14]. All these properties and abilities along with the fact that GNPs, as other metal nanoparticles, are amenable to the attachment of biomolecules or ligands through well-known thiol and amino chemistry or simply by electrostatic interactions [15–17] have led to a wealth of nanoparticle-based optical bio-sensing approaches for many applications. The majority of them have been concerned with measurements of the plasmon absorption, monitored by direct absorption or even by simply analyzing the visual color, and its modifications induced either by changes of dielectric properties of the medium surrounding the gold surface, due to the presence of molecules in the proximity of the surface, or by aggregation and flocculation of the nanoparticles in solution [18–25]. Since the plasmon resonance can also be involved in a modulation of the electric field around the nanoparticle giving rise to the enhancement of Raman scattering or fluorescence signal of nearby molecules [26,27], GNP-based biosensors exploiting fluorescence or Raman effects have also been developed and used [28,29]. In recent times, also the ability of metallic nanoparticles to efficiently scatter light [1,2,5,13,14] has received attention and several groups have reported about the use of GNPs in biomolecular assays based on GNP scattering properties [30–36], using the approach of inducing nanoparticle aggregation by the target molecule as to have a huge change in sample light scattering properties. Resonance Light Scattering (RLS) is a technique which exploits the increase of scattering efficiency occurring when the incident beam is close in wavelength to the plasmon absorption band. This phenomenon is amplified when nanoparticles giving rise to the plasmon band are strongly coupled (as occurs when particles form aggregates) and hence RLS is particularly well-suited for studying processes in which nanoparticles aggregate. Accordingly, it has been successfully applied to investigate a large variety of systems including porphyrin [37,38], dye—nucleic acids [39] and dye—protein [40–42] aggregates. Aslan et al. have used changes in RLS signal to detect glucose [43]. They have also demonstrated the efficiency of an angular-ratiometric light scattering method in sensing nanoparticle aggregation [44] in which the angular distribution of scattered light from different sized nanoparticles has been utilized for sensing. More recently, Huo et al. [45,46] have introduced a new approach by switching to detect particle size change for quantifying the content of the target analyte in liquid samples as a consequence of the induced GNP probe aggregation, using Dynamic Light Scattering (DLS) [47] technique. This approach has been shown to efficiently detect Human IgG protein in the 1.6–25 μg/ml range [36,48].

Despite the increasing use of light scattering methods for realizing nanoparticle aggregation-based sensing approaches, no systematic comparison among these methods has been performed till now. Static and Dynamic Light Scattering (SLS and DLS, respectively) along with Resonance Light Scattering (RLS) and angular-ratiometric methods are here compared using the probe-aggregation approach for better elucidating the effect of analyte-induced nanoparticle aggregation on the scattered intensity-depending signals. The comparison has been carried on by exploiting the characteristics of a well defined and well-known model system, i.e., biotin and one of its partners, neutravidin. The specific interaction of biotin with avidin, streptavidin and neutravidin, which is characterized by an extremely high binding affinity, $K \approx 10^{13}\ M^{-1}$ [49], has been widely used to test sensing approaches based on analyte-induced nanoparticle aggregation. In fact, neutravidin is a tetrameric protein, which can bind up to four biotinylated-bovine serum albumin (BSA) molecules. For these reasons, neutravidin has been used to induce the aggregation of biotinylated-BSA-coated GNPs (BBSA-GNPs). The study of neutravidin induced aggregation of BBSA-GNPs by the selected light scattering methods has enabled to obtain at the same time information on dependence of the scattered intensity on the scattering angle (obtained by SLS) and on the wavelength of the incident light (by RLS) along with an estimation of the hydrodynamic size of the nanoparticle aggregates (by DLS). These results along with information obtained by applying the angular-ratiometric approach have been compared with Mie theory predictions and discussed also in the view of the potentials of the light scattering methods in biosensing.

2. Materials and methods

2.1. Sample preparation

2.1.1. Materials

Gold nanoparticle (20 nm) solution was purchased from Ted Pella. Sodium phosphate monobasic, phosphate buffered saline (PBS), neutravidin, and biotinamidocaproyl labeled bovine serum albumin (biotinylated BSA) were purchased from Sigma-Aldrich. All chemicals were used as received.

2.1.2. Preparation of biotinylated BSA-coated 20 nm gold nanoparticles

The surface modification of 20 nm gold nanoparticles was performed using the procedure described in Ref. [44]. Briefly, 5 ml of the gold nanoparticle solution was mixed with 0.05 ml of aqueous solution of biotinylated BSA (1.44 mg/ml), and this mixture was incubated at room temperature for 2 h. In this way, BSA molecules are in excess with respect to the number of particles that can be host on the gold nanoparticles (around 25 biotin-BSA molecules are enough to cover the surface of a 20-nm nanoparticle). The GNP/biotinylated BSA mixture was then centrifuged in an Eppendorf centrifuge tube equipped with a 100,000 MW cutoff filter for 10 min, using an Eppendorf microcentrifuge at 8000 *g*, to separate the biotinylated BSA-coated GNPs from the excess biotinylated BSA. The supernatant was carefully removed, and the pellet containing the biotinylated gold nanoparticles was resuspended in 10 mM sodium phosphate buffer (pH 7). The resulting solution was subsequently used in the aggregation procedure, without applying any additional procedure.

2.1.3. Aggregation procedure by using biotinylated gold nanoparticles and neutravidin

The aggregation was induced by mixing biotinylated gold nanoparticles with increasing concentrations of neutravidin in a quartz cuvette. In this regard, a 3.3 μM stock solution of neutravidin was prepared in PBS based buffer. To achieve the desired final neutravidin concentrations ($c = 0, 5, 10, 18, 25$ nM), successive predetermined volumes of neutravidin stock solution were used and incubated for 90 min at each addition step. The scheme of the model system investigated is reported in Fig. 1a. The depicted process envisages the occurrence of the binding between biotin (available on GNP surface) and neutravidin (given the value $K \approx 10^{13}\ M^{-1}$, it is well known that harsh conditions are required to break the formed bond) leading to the formation of nanoparticle aggregates, in agreement with previous literature reports [44].

Absorption spectra of the solutions were recorded after each step of the sample preparation and the aggregation procedures by using a Jasco dual-beam spectrophotometer Model UV–vis 550 and placing the suspensions in a quartz cuvette. The detected spectra (Fig. 1b) confirmed both the completion of biotin-BSA adsorption on the GNPs and GNP aggregation due to neutravidin addition.

2.2. Methods

2.2.1. Resonance Light Scattering

RLS spectra were collected in the 250–800 nm range at room temperature by a Spex FluoroMax (Jobin Yvon, France) spectrofluorometer, equipped with 450 W Xenon lamp and two monochromators. The spectrofluorometer was used in synchroscan mode with the same excitation and emission wavelength ($\Delta\lambda = 0$). The bandpass width for the excitation and emission monochromators was 2.0 nm. Preliminary measurements with two polarizers (one placed on the exciting light path and the other after the sample on the emitted light path) performed on

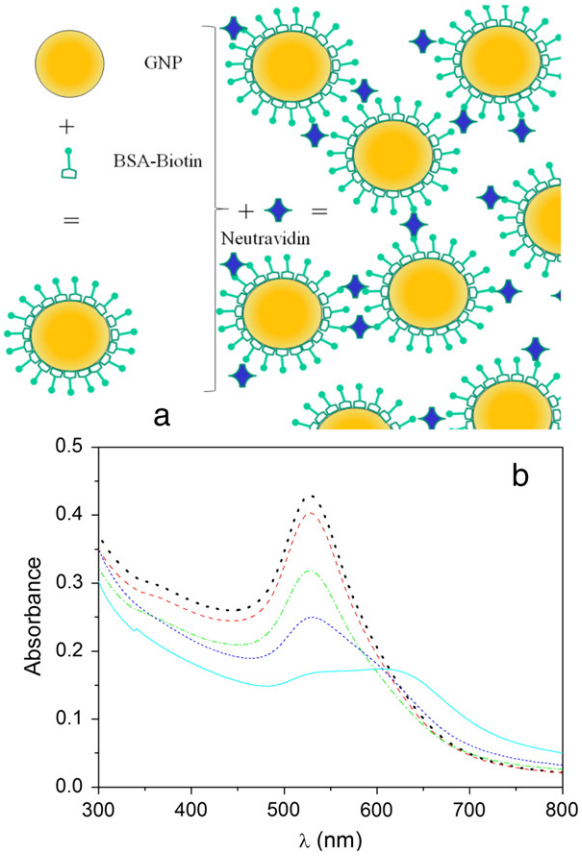

Fig. 1. (a) Schematic drawing of investigated model system (Biotin-BSA nanoparticles aggregating upon neutravidin addition). (b) absorption spectra of Biotin-BSA 20-nm gold nanoparticle solutions at different neutravidin concentrations; black dotted line: c = 0 nM, red dashed line: c = 5 nM; green dash dotted line c = 10 nM; blue short-dashed line c = 18 nM; cyan continuous line c = 24 nM.

bare GNP solutions allowed us to define the experimental conditions providing the best signal-to-noise ratio. Accordingly, a configuration with the first polarizer perpendicular to the scattering plane and the other one parallel to the same plane was used. An integration time of 1.0 s, that relates to 0.5 nm step, was used. The light emitted by each sample kept in a 1.0 cm × 1.0 cm internal size quartz cuvette was collected at right angle to the excitation radiation. RLS spectra were corrected for variations in lamp intensity by dividing the sample signal intensity by the reference intensity (recorded by Spex photodiode detector).

2.2.2. Static and Dynamic Light Scattering

SLS and DLS measurements were performed by using an apparatus equipped with an Argon laser (working at 488 nm; laser maximum power of 30 mW), a commercial Brookhaven Instrument BI-9836 photomultiplier tube (PMT), two polarizers (one, Pol A, was placed on the path of the incident light, and the other, Pol B, on the path of the detected light), collecting lenses, a pinhole with variable dimensions, and a Brookhaven Instrument BI-9000 digital correlator. The PMT was mounted on a motorized holder connected to a Brookhaven Instrument BI-200 goniometer. In the employed set-up, the horizontal plane, in which both the PMT and the laser lie and including the scattering volume, is the scattering plane (in fact the scattering plane is defined as the plane in which both the vector of the detector position and the direction of the incident beam lie).

In SLS measurements, scattered intensity was automatically acquired at 22 angles in the range 30–140° with a 5°-step. The pinhole dimension and the acquisition time were defined in order to optimize the signal-to-noise ratio and intensity stability for a sample used for reference, namely, pure nanoparticle solution (GNP concentration 0.6 nM). Various sets of angle dependent intensities were collected for each investigated sample with polarizers in two detection configurations (PERP configuration: Pol A and Pol B set perpendicular to the scattering plane; PAR configuration: Pol A and Pol B set parallel to the scattering plane).

In DLS measurements, autocorrelation function of the light intensity detected at 90° scattering angle was recorded by the correlator with polarizers set in PERP detection configuration. The pinhole dimension and the acquisition time were defined for each experimental configuration in order to optimize the signal-to-noise ratio and intensity stability for the reference sample. The temperature of the sample was kept at 25.0 ± 0.5 °C by a thermostatic bath.

2.3. Data analysis and Mie calculations

2.3.1. Static Light Scattering data analysis

The light scattered by very small subwavelength sized particles is well described by Rayleigh theory [1,2,13]. Accordingly, it is well known that for incident light of wavelength λ horizontally polarized with respect to the scattering plane and observed in the same plane, the intensity of light scattered by a homogeneous spherical particle with radius a, being a ≪ λ, in the direction θ is given by the Rayleigh expression [1,2,13],

$$I_{PAR} = \frac{16\pi^4 a^6 n^4 I_0}{r^2\lambda^4}\left|\frac{n_1^2-1}{n_1^2+2}\right|\cos^2\theta \quad (1)$$

where I_0 is the incident intensity of the monochromatic light, n is the refractive index of the medium surrounding the particle, n_1 is the refractive index of the bulk particle material and r is the distance between the particle and the position where the scattered light is detected. For larger particles, i.e., for particles with a > 1/20 λ, or for small particles in close proximity to one another, the scattering process is no longer described by Rayleigh theory (Eq. (1)) but indeed can be depicted by Mie theory [13,14], which provides the extinction cross section and intensity of scattered light at defined scattering angles for spherical GNPs of known diameter.

Given the geometry of the scattering apparatus, the direct inspection of I_{PAR} vs θ profiles was used to study the scattering regime of the sample. Actually, the particle radius and the laser wavelength were chosen to follow the transition between Rayleigh and Mie scattering regimes eventually occurring after neutravidin induced biotin-BSA-coated GNP aggregation. The experimental angular intensity profiles were compared with results from Mie theory predictions.

I_{PERP} vs θ profiles were instead used to define the best angles for applying the angular-ratiometric approach [44] which consists in monitoring nanoparticle aggregation by the analysis of the ratio of the scattered intensity at two angles. In this way the increase in absolute scattered intensity is exploited and the result is get rid by intensity fluctuations. For an optimal efficiency of the method, one of the angles (θ_2) has to be characterized by a significant dependence of scattered intensity on GNP radius and the other (θ_1) is used to have a reference intensity. After having defined the best θ_1 and θ_2 angles, the value of $I(\theta_2)/I(\theta_1)$ was obtained for each samples and studied as a function of neutravidin concentration.

2.3.2. Dynamic Light Scattering data analysis

DLS measurements provide the autocorrelation function of the scattered intensity vs time delay (τ) at a well defined scattering angle [47,50]. For an ideal sample (i.e., an infinite dilute sample in which scattering objects undergo only a translational diffusion process), the correlation function can be described as [47,50–52]

$$g(q,\tau) = 1 + \exp(-2\Gamma\tau) \quad (2)$$

where Γ is the decay rate. The Γ value for the scattered light having the same polarization as the incident beam is expressed as $\Gamma = Dq^2$, where D is the translational diffusion coefficient, and $q = 2\pi n/\lambda \sin(\theta/2)$. The analysis of the correlation function was performed by applying Multiexponential Sampling method [53]. The resulting values of Γ parameter can be used to obtain the experimental estimation of D and, under the additional hypothesis of spherical particles, information on the absolute value of the particle hydrodynamic diameter (d_h) by using Stokes–Einstein relation [47,51]

$$d_h = \frac{K_B T}{3\pi\eta D} \tag{3}$$

where K_B is the Boltzmann constant, T the absolute temperature and η the viscosity of the medium.

2.3.3. Mie calculations

Predictions about the intensity of the scattered light parallel ($i_\parallel$) and perpendicular ($i_\perp$) to the scattering plane were obtained according to Mie theory [13,14] for different sized spherical gold nanoparticles in water at 25 °C by MiePlot software pack [54]. In particular $i_\parallel$ was calculated as $i_\parallel = |S_2|^2$ and $i_\perp$ was calculated as $i_\perp = |S_1|^2$ where [13]

$$S_1 = \sum_{m=1}^{\infty} \frac{2m+1}{m(m+1)}(a_m \pi_m + b_m \tau_m) \tag{4a}$$

$$S_2 = \sum_{m=1}^{\infty} \frac{2m+1}{m(m+1)}(a_m \tau_m + b_m \pi_m) \tag{4b}$$

with a_m and b_m coefficients calculated as follows

$$a_m = \frac{N\psi_m(Nx)\psi'_m(x) - \psi_m(x)\psi'_m(Nx)}{N\psi_m(Nx)\xi'_m(x) - \xi_m(x)\psi'_m(Nx)} \tag{5a}$$

$$b_m = \frac{\psi_m(Nx)\psi'_m(x) - N\psi_m(x)\psi'_m(Nx)}{\psi_m(Nx)\xi'_m(x) - N\xi_m(x)\psi'_m(Nx)} \tag{5b}$$

where $N = n/n_1$, n_1 is the refractive index of the bulk particle material, $x = ka$, a is the particle radius, $k = \frac{2\pi n}{\lambda}$, λ is the incident light wavelength, $\psi_m(\rho) = \rho j_m(\rho)$ and $\xi_m(\rho) = \rho h_m^{(1)}(\rho)$ are the Riccati–Bessel functions. τ_m and π_m are related to the first derivative of the Legendre polynomials (P_m^1) as the following:

$$\pi_m = \frac{P_m^1}{\sin\theta}; \qquad \tau_m = \frac{dP_m^1}{d\theta}.$$

The calculations were performed using the data for gold and water refractive indexes provided by the software package (for water, Segelstein data at 20 °C were used) [54].

3. Results and discussion

3.1. Resonance Light Scattering

The RLS spectra as detected from Biotin-BSA 20-nm GNP (BBSA-GNP) solutions without and with neutravidin at various concentrations are shown in Fig. 2a. All the spectra feature two peaks at 377 and 555 nm. The latter peak is the highest one and is spectrally close to the plasmon resonance peak, to which it can be related. As the neutravidin concentration increases, the absolute RLS intensity decreases and the relative intensity of the peaks changes. This confirms that RLS approach is able to monitor the process induced by biotin–neutravidin interaction. To quantify the signal variation, the integral (Integral(c)) of each spectrum has been calculated and the difference between the value obtained at c = 0 and those at c has then been obtained. The quantity |Δ(Spectrum Integral)| = Integral(c = 0) − Integral(c) has been extracted for each

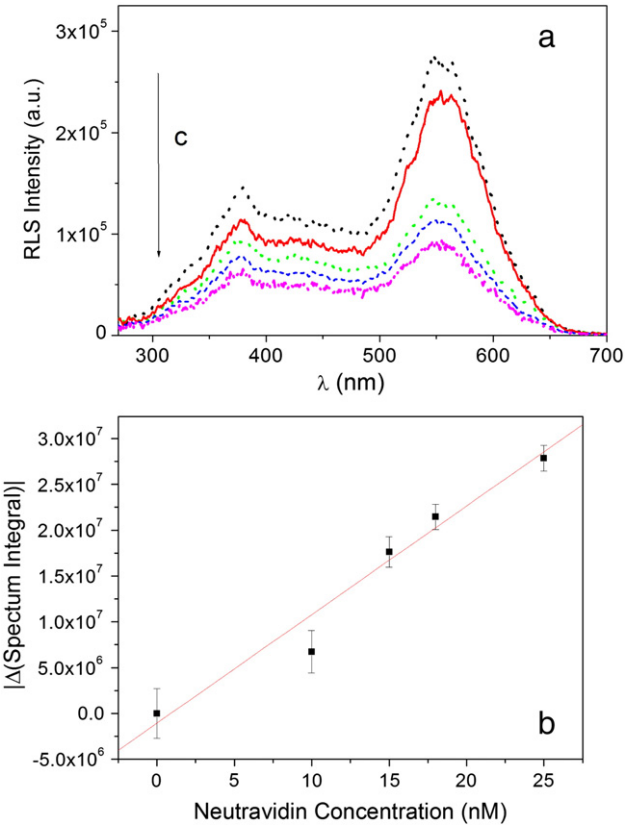

Fig. 2. (a) RLS spectra of Biotin-BSA 20-nm gold nanoparticle solutions at different neutravidin concentrations (c = 0, 10, 15, 20, 25 nM, shown as black dotted, red continuous, green dashed, blue short-dashed, magenta dash–dot-dotted lines, respectively). (b) Values of the spectrum integral from RLS spectra. Red line: curve resulting from a weightened linear fitting procedure y = a + bx, with a = (−1.1 ± 2.0) 10^6 a.u. and b = (1.19 ± 0.11) 10^6 a.u./nM, r = 0.984.

neutravidin concentration. The resulting values are shown in Fig. 2b. As is evident, they linearly increase with neutravidin concentration, enabling the use of a linear fitting procedure (parameters reported in the figure caption). The resulting slope of the curve is of (1.19 ± 0.11) 10^6 nM^{-1} suggesting a possible sensitivity in detecting neutravidin in the order of 10^{-6} nM^{-1}.

3.2. Static Light Scattering and ratiometric approach

The angular scattering profiles (I_{PAR} vs θ) obtained for BBSA-GNP solutions at increasing neutravidin concentrations are shown in Fig. 3. The scattering profile changes from a relatively simple Rayleigh ($\cos^2\theta$) behavior in the absence of neutravidin to a more complex behavior when neutravidin is added in solution. Notably, an increase in forward (θ = 0°) scattering intensity with increasing neutravidin concentration is observed. These findings are consistent with a change from Rayleigh to Mie scattering, thus confirming the occurrence of nanoparticle aggregation process induced by neutravidin–biotin interaction, similarly to what was found for streptavidin–biotin model assay system [43,44]. This is further confirmed by the comparison of the angular scattering profile of the solutions and angular dependence of Mie scattering cross section for particles of two different diameters: 20 and 130 nm, shown as lines in Fig. 3. The Mie theory estimations for the 20-nm and 130-nm diameter particles have the same profile as the scattering data obtained at low and high neutravidin concentrations, respectively, thus witnessing that the outlined changes in the scattering profile can be related to the change in size of the aggregates.

I_{PERP} vs θ profiles have been used to define the best angles for applying the angular ratiometric approach, as described in Section 2.3.

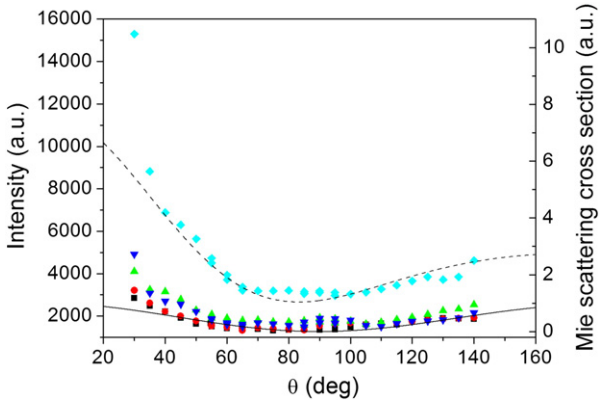

Fig. 3. Angular dependent scattering from 20-nm BSA-biotin gold nanoparticle solutions at various neutravidin concentrations (c = 0, 5, 10, 18, 25 nM, shown as black square, red rumble, green up triangle, blue down triangle, and cyan diamond, respectively) as obtained in PAR detection configuration. Lines represent results of Mie calculation for gold spherical particle with 20 (continuous line) and 130 nm (dotted line) diameter; the vertical scale for lines being the left scale.

Accordingly, the angular dependent scattering profiles shown above make reasonable to investigate the ratio of the scattered intensity at 40° and 90°. The value of this ratio has been calculated for each sample and the results are shown in Fig. 4 as a function of neutravidin concentration. As it comes clear, the I_{40}/I_{90} intensity ratio increases with neutravidin concentration, in agreement with previous reports [44]. In particular, it can be noticed that the ratio features an exponential dependence on neutravidin concentration (c), i.e., $I_{40}/I_{90} = y_0 + A\exp(c/B)$, as witnessed by the curve resulting from a fitting procedure shown as red line in the figure, suggesting a high sensitivity of the ratio to neutravidin concentration. For comparison, the I_{40}/I_{90} ratios calculated using Mie scattering cross sections obtained for particles of increasing radius are shown in the same figure (see dashed line). The calculated ratios feature a dependence on the diameter of the scattering object similar to that observed for I_{40}/I_{90} vs neutravidin concentration. This confirms that also the I_{40}/I_{90} ratio is sensitive to the presence of neutravidin and the observed changes can be directly related to changes in the size of the scattering objects and, thus, on the degree of aggregation of nanoparticles induced by the interaction between neutravidin and biotin.

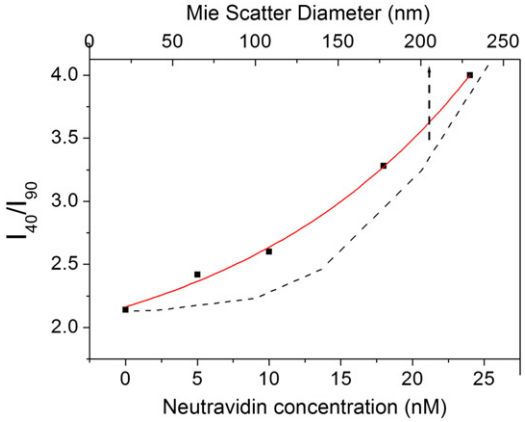

Fig. 4. I_{40}/I_{90} scattered PERP intensity ratio from aggregated BSA-biotin colloids as a function of neutravidin concentration and corresponding curve resulting from an exponential growth regression (red continuous line). Dashed black line: I_{40}/I_{90} scattered PERP intensity ratios as predicted by Mie theory for different sized gold scattering objects; diameter being shown in the upper horizontal scale.

3.3. Dynamic Light Scattering

Autocorrelation functions as obtained by using DLS for investigating Biotin-BSA 20-nm gold nanoparticle solutions with increasing neutravidin concentrations are shown in Fig. 5a. It can be observed that the decay time of the function increases with neutravidin concentration, resulting in a decrease in the Γ parameter introduced in Eq. (2). Since $\Gamma = Dq^2$, this decrease has to be due to a reduction of the diffusion coefficient of the scattering objects, D, being q fixed by the employed experimental conditions. Under dilute conditions, for an object undergoing a translational diffusion motion in a fluid at fixed temperature, T, a decrease in the diffusion coefficient has to result from an increase in either the hydrodynamic diameter of the scattering object or the fluid viscosity (see Eq. (3)). In the present case, a simplified picture is used to take into account that the aggregates cannot be considered as perfect geometrical spheres and that both the interparticle interaction and biomolecule–biomolecule interactions could affect the motion of the scattering objects. In particular, all the effects due to neutravidin addition in solution are here thought to affect only the value of the hydrodynamic diameter of the aggregates, that is read as an apparent diameter; the fluid viscosity is considered to be constant over the investigated neutravidin concentration range. In this framework, the reduction of the diffusion coefficient is ascribed to an increase in the hydrodynamic diameter of the aggregates. To quantify this increase an analysis of the autocorrelation functions by means of Multiexponential Sampling fit method has been carried out, providing the distribution of the size of the aggregates shown in Fig. 5b. The obtained histograms

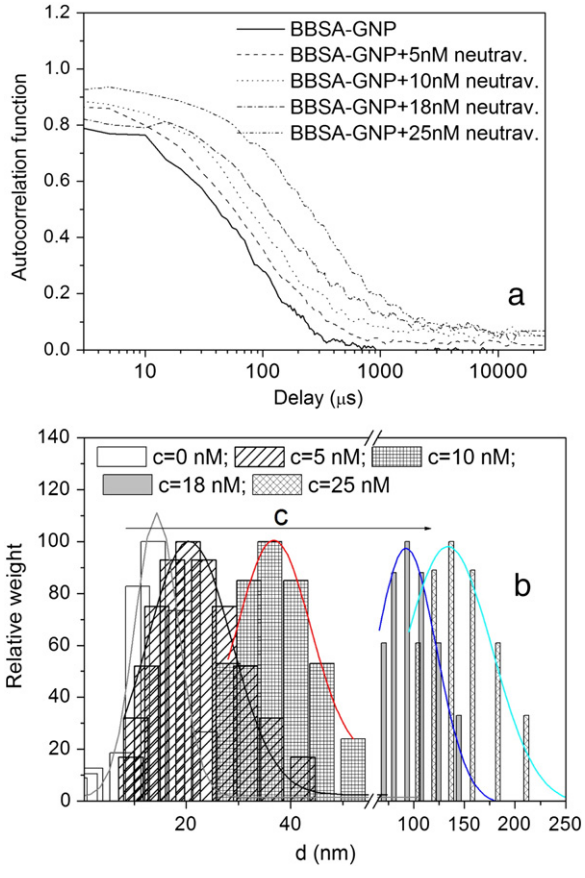

Fig. 5. (a) Autocorrelation functions of light scattered at 90° (T = 25 °C) from Biotin-BSA 20-nm gold colloid solutions with increasing neutravidin concentrations (c = 0, 10, 18, 25 nM, shown as continuous, dashed, dotted, dash-dotted, and dash–dot dotted lines, respectively); temporal range 3–20,000 μs. (b) Diameter distributions resulting from Multiexponential Sampling method fit applied to autocorrelation functions and corresponding Gaussian fit functions (continuous lines).

have then been fitted by Gaussian distributions whose central values and width parameters are the following: 24 ± 8 nm, 27 ± 16 nm, 37 ± 14 nm, 92 ± 60 nm, and 134 ± 80 nm, for 0, 5, 10, 18 and 25 nM neutravidin concentration, respectively. The observed size of the aggregates increases with neutravidin concentration. This evidence along with literature reports [44] and the above discussed results confirm the occurrence of the aggregation process and provide an indicative size of the formed aggregates.

The overall analysis of the data obtained by all the employed light scattering methods confirms that they are all sensitive to the presence of neutravidin which induces the aggregation of the nanoparticle probes. The availability of the data on the size of the aggregates obtained by DLS allows us to correlate the detected changes in I_{40}/I_{90} ratio and in RLS integrated intensity to a change in the size of the scattering objects. In fact, the I_{40}/I_{90} ratio dependence on neutravidin concentration has been compared to the Mie extinction efficiency of nanoparticle of increasing sizes.

Even if providing information for the realization of a specific biosensor is out of the scope of the present work, the described results can be analyzed for evaluating the potentials of each scattering-based method for sensing target biomolecules in the nM-concentration range. At this aim, a qualitative comparison among the response ability of the investigated methods can be done considering the relative signal changes at the different investigated neutravidin concentrations by calculating the quantity

$$\frac{\Delta S}{S} = \frac{|S(c) - S(0)|}{S(0)} \tag{6}$$

where S(c) is the signal detected (i.e., central value of the Gaussian distribution of the size for DLS, I_{40}/I_{90} value for angular ratiometric approach and integral of the spectrum for RLS) at the neutravidin concentration c and S(0) is S(c) at c = 0 (no neutravidin in BBSA-GNP solution). The resulting values are reported in Fig. 6 and make clear that the highest relative variation of the signal at the highest neutravidin concentration is obtained by DLS, suggesting that this technique could offer the best sensitivity. This can be explained considering that the signal extracted from DLS (i.e., the apparent size of the aggregates) is the only one that is sensitive to all the effects due to neutravidin addition, including changes in the size and in the characteristics of the motions of the aggregates. Among the other methods, the highest variation is obtained when the integral of the RLS spectrum is used to monitor neutravidin induced particle aggregation. In addition, the RLS signal shows a linear dependence on the target molecule concentration, thus it can be directly used for monitoring neutravidin concentration in the investigated concentration range. The ratiometric approach potentially has a very high sensitivity according to the observed exponential dependence of the signal on neutravidin concentration. However, a more accurate calibration would be required in a sensing method eventually based on such an approach. Despite the outlined differences, all the methods have shown to be sensitive to neutravidin present in solution in nM-concentration range. Given the high dependence of the scattering properties of nanoobjects on their size, shape, and geometry and considering the continuously increasing ability in tailoring these properties, this evidence suggests that light scattering-based methods have the potentials to reach a sensitivity comparable to those reported, for similar systems, for other optical approaches, resulting in picomolar range for colorimetric, fluorescence and Surface-Enhanced Raman scattering-based methods [25,28,29].

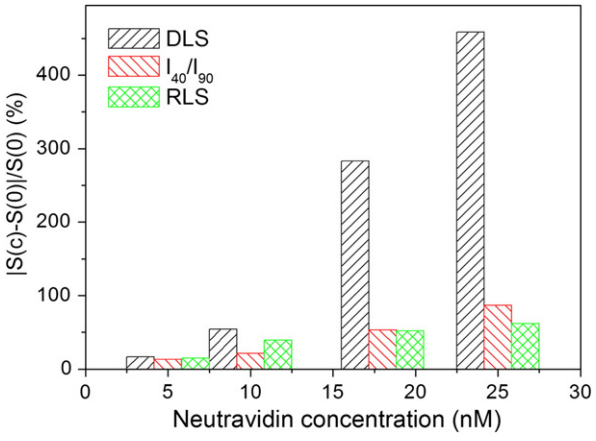

Fig. 6. Values of the ΔS/S (see text) for the methods employed for investigating nanoparticle aggregation.

4. Conclusions

The study of aggregation of Biotin-BSA coated 20-nm gold nanoparticles by SLS, DLS, RLS and angular-ratiometric methods confirmed that all the approaches are able to sense the presence in solution of neutravidin at concentrations in the nanomolar range. The availability of information on both apparent aggregate size of the aggregates and angular distribution of scattered light intensity along with numerical evaluation of the scattered light intensity profile by using Mie theory allowed us to relate the outlined modifications in the scattering properties to changes in scatter size, thus strengthening the comprehension of the dependence of the signals on the characteristics of the sample. The results were also discussed in the view of the possible use of the employed methods for sensing applications. It came out that the greatest changes in the signal used for monitoring aggregation were obtained by DLS. A linear dependence on neutravidin concentration was outlined only for RLS signal, while the signal used in ratiometric approach showed an exponential-type dependence on the analyte concentration. These evidences suggest that RLS can be simply used as sensing method to quantify an analyte; on the contrary the ratiometric approach would require a more accurate calibration to realize a sensing method eventually based on such an approach. These results are a good starting point for future work aimed at evaluating the limits and advantages (in terms of limit of detection, specificity, easiness of use, versatility) of each technique, which would further widen the use of light scattering methods for biosensing.

References

[1] J. Yguerabide, E.E. Yguerabide, Light-scattering submicroscopic particles as highly fluorescent analogs and their use as tracer labels in clinical and biological applications, Analytical Biochemistry 262 (1998) 137–156.
[2] J. Yguerabide, E.E. Yguerabide, Light-scattering submicroscopic particles as highly fluorescent analogs and their use as tracer labels in clinical and biological applications: II. Experimental characterization, Analytical Biochemistry 262 (1998) 157–176.
[3] K.L. Kelly, E. Coronado, L.L. Zhao, G.C. Schatz, The optical properties of metal nanoparticles: the influence of size, shape, and dielectric environment, The Journal of Physical Chemistry. B 107 (2003) 668–677.
[4] V. Degiorgio, R. Piazza, Light scattering in colloid and interface science, Current Opinion in Colloid and Interface Science 1 (1996) 11–16.
[5] R. Sardar, A.M. Funston, P. Mulvaney, R.W. Murray, Gold nanoparticles: past, present, and future, Langmuir 25 (2009) 13840–13851.
[6] K. Kneipp, H. Kneipp, I. Itzkan, R.R. Dasari, M.S. Feld, Ultrasensitive chemical analysis by Raman spectroscopy, Chemical Reviews 99 (1999) 2957–2976.
[7] I. Delfino, A.R. Bizzarri, S. Cannistraro, Single-molecule detection of yeast cytochrome c by surface-enhanced Raman spectroscopy, Biophysical Chemistry 113 (2005) 41–51.
[8] I. Delfino, A.R. Bizzarri, S. Cannistraro, Time-dependent study of single-molecule SERS signal from yeast cytochrome c, Chemical Physics 326 (2006) 356–362.
[9] S.E. Lohse, C.J. Murphy, Applications of colloidal inorganic nanoparticles: from medicine to energy, Journal of the American Chemical Society 134 (2012) 15607–15620.
[10] K. Saha, S.S. Agasti, C. Kim, X. Li, V.M. Rotello, Gold nanoparticles in chemical and biological sensing, Chemical Reviews 112 (2012) 2739–2779.
[11] A. Liang, Q. Liu, G. Wen, Z. Jiang, The surface-plasmon-resonance effect of nanogold/silver and its analytical applications, TRAC Trends in Analytical Chemistry 37 (2012) 32–47.
[12] P.K. Jain, K.S. Lee, I.H. El-Sayed, M.A. El-Sayed, Calculated absorption and scattering properties of gold nanoparticles of different size, shape, and composition:

applications in biological imaging and biomedicine, The Journal of Physical Chemistry. B 110 (2006) 7238–7248.
[13] C.F. Bohren, D.R. Huffman, Absorption and Scattering of Light by Small Particles, John Wiley & Sons, Inc., New York, 1983.
[14] G. Mie, Beiträge zur Optik trüber Medien, speziell kolloidaler Metallösungen, Annalen der Physik 25 (1908) 377–445.
[15] I. Delfino, S. Cannistraro, Optical investigation of the electron transfer protein azurin–gold nanoparticle system, Biophysical Chemistry 139 (2009) 1–7.
[16] L. Venkataraman, J.E. Klare, I.W. Tam, C. Nuckolls, M.S. Hybertsen, M.L. Steigerwald, Single-molecule circuits with well-defined molecular conductance, Nano Letters 6 (2006) 458–462.
[17] J. Gao, X. Huang, H. Liu, F. Zan, J. Ren, Colloidal stability of gold nanoparticles modified with thiol compounds: bioconjugation and application in cancer cell imaging, Langmuir 28 (2012) 4464–4471.
[18] V. Amendola, M. Meneghetti, Size evaluation of gold nanoparticles by UV–vis spectroscopy, Journal of Physical Chemistry C 113 (2009) 4277–4285.
[19] K.S. Mayya, V. Patil, M. Sastry, On the stability of carboxylic acid derivatized gold colloidal particles: the role of colloidal solution pH studied by optical absorption spectroscopy, Langmuir 13 (1997) 3944–3947.
[20] R.A. Reynolds, C.A. Mirkin, R.L. Letsinger, Homogeneous, nanoparticle-based quantitative colorimetric detection of oligonucleotides, Journal of the American Chemical Society 122 (2000) 3795–3796.
[21] C.A. Mirkin, R.L. Letsinger, R.L. Mucic, J.J. Storhoff, A DNA-based method for rationally assembling nanoparticles into macroscopic materials, Nature 382 (1996) 607–609.
[22] Y. Kim, R.C. Johnson, J.T. Hupp, Gold nanoparticle-based sensing of "spectroscopically silent" heavy metal ions, Nano Letters 1 (2001) 165–167.
[23] S.Y. Lin, S.W. Liu, C.M. Lin, C.H. Chen, Recognition of potassium ion in water by 15-crown-5 functionalized gold nanoparticles, Analytical Chemistry 74 (2002) 330–335.
[24] N.T.K. Thanh, Z. Rosenzweig, Development of an aggregation-based immunoassay for anti-protein A using gold nanoparticles, Analytical Chemistry 74 (2002) 1624–1628.
[25] S. Lim, O.K. Koo, Y.S. You, Y.E. Lee, M.-S. Kim, P.-S. Chang, D.H. Kang, J.-H. Yu, Y.J. Choi, S. Gunasekaran, Enhancing nanoparticle-based visible detection by controlling the extent of aggregation, Scientific Reports 2 (2012) 456/1-6.
[26] K. Kneipp, H. Kneipp, I. Itzkan, R.R. Dasari, M.S. Feld, Ultrasensitive chemical analysis by Raman spectroscopy, Chemical Reviews 99 (1999) 2957–2975.
[27] J.R. Lakowicz, J. Kusba, Y. Shen, J. Malicka, S. D'Auria, Z. Gryczynski, I. Gryczynski, Effects of metallic silver particles on resonance energy transfer between fluorophores bound to DNA, Journal of Fluorescence 13 (2003) 69–77.
[28] J. Yao, X. Han, S. Zeng, W. Zhong, Detection of femtomolar proteins by non-fluorescent ZnS nanocrystal clusters, Analytical Chemistry 7 (84) (2012) 1645–1652.
[29] F. Domenici, A.R. Bizzarri, S. Cannistraro, Surface-enhanced Raman scattering detection of wild-type and mutant p53 proteins at very low concentration in human serum, Analytical Biochemistry 421 (2012) 9–15.
[30] B.-A. Du, Z.-P. Li, C.-H. Liu, One-step homogeneous detection of DNA hybridization with gold nanoparticle probes by using a linear light-scattering technique, Angewandte Chemie International Edition 45 (2006) 8022–8025.
[31] P.C. Ray, Diagnostics of single base-mismatch DNA hybridization on gold nanoparticles by using the hyper-Rayleigh scattering technique, Angewandte Chemie International Edition 45 (2006) 1151–1154.
[32] H. Xie, K.L. Gill-Sharp, D.P. Oneal, Quantitative estimation of gold nanoshell concentrations in whole blood using dynamic light scattering, Nanomedicine: Nanotechnology, Biology and Medicine 3 (2007) 89–94.
[33] L.R. Hirsch, J.B. Jackson, N.J. Halas, J.L. West, A whole blood immunoassay using gold nanoshells, Analytical Chemistry 75 (2003) 2377–2381.
[34] K. Aslan, J.R. Lakowicz, C.D. Geddes, Angular-dependent polarization-based plasmon light-scattering for bioaffinity sensing, Applied Physics Letters 87 (2005), [234108/1-234108/3].
[35] V. Román-Pizarro, J.M. Fernández-Romero, A. Gómez-Hens, Gold nanoparticle-biotinylated liposome hybrids as analytical reagents for biotin determination using a competitive assay and resonance light scattering detection, Talanta 99 (2012) 538–543.
[36] X. Wang, Y. Li, D. Quan, J. Wang, Y. Zhang, J. Du, J. Peng, Q. Fu, Y. Zhou, S. Jia, Y. Wang, L. Zhan, Detection of hepatitis B surface antigen by target-induced aggregation monitored by dynamic light scattering, Analytical Biochemistry 428 (2012) 119–125.
[37] R.F. Pasternack, P. Schaefer, P. Hambright, Resonance light-scattering studies of porphyrin diacid aggregates, Inorganic Chemistry 33 (1994) 2062–2065.
[38] R.F. Rubires, J. Crusats, Z. El-Hachemi, T. Jaramillo, M. Lopez, E. Valls, J.-A. Farrera, J.M. Ribo, Self-assembly in water of the sodium salts of meso-sulfonatophenyl substituted porphyrins, New Journal of Chemistry 23 (1999) 189–198.
[39] Y.F. Li, W.Q. Shu, P. Feng, C.Z. Huang, M. Li, Determination of DNA with cetyltrimethylammonium bromide by the measurement of resonance light scattering, Analytical Sciences 17 (2001) 693–696.
[40] Q.E. Cao, Z.T. Ding, R.B. Fang, X. Zhao, A sensitive and rapid method for the determination of protein by the resonance Rayleigh light-scattering technique with pyrogallol red, Analyst 126 (2001) 1444–1448.
[41] L.Y. Wang, L. Wang, L. Dong, Y.L. Hu, T.T. Xia, H.Q. Chen, L. Li, C.Q. Zhu, Determination of γ-globulin at nanogram levels by its enhancement effect on the resonance light scattering of functionalized HgS nanoparticles, Talanta 62 (2004) 237–240.
[42] C.Z. Huang, C.X. Yang, Y.F. Li, Determination of proteins with Ponceau G by compensating for the molecular absorption decreased resonance light scattering signals, Analytical Letters 36 (2003) 1557–1571.
[43] K. Aslan, J.R. Lakowicz, C.D. Geddes, Nanogold plasmon resonance-based glucose sensing. 2. Wavelength-ratiometric resonance light scattering, Analytical Chemistry 77 (2004) 2007–2014.
[44] K. Aslan, P. Holley, L. Davies, J.R. Lakowicz, C.D. Geddes, Angular-ratiometric plasmon resonance light scattering for bioaffinity sensing, Journal of the American Chemical Society 127 (2005) 12115–12121.
[45] X. Liu, Q. Dai, L. Austin, J. Coutts, G. Knowles, J. Zou, H. Chen, Q. Huo, A one-step homogeneous immunoassay for cancer biomarker detection using gold nanoparticle probes coupled with dynamic light scattering, Journal of the American Chemical Society 130 (2008) 2780–2782.
[46] Q. Dai, X. Liu, J. Coutts, L. Austin, Q. Huo, A one-step highly sensitive method for DNA detection using dynamic light scattering, Journal of the American Chemical Society 130 (2008) 8138–8139.
[47] B.J. Berne, R. Pecora, Dynamic Light Scattering, Wiley-Interscience, New York, 1976.
[48] H. Jans, X. Liu, L. Austin, G. Maes, Q. Huo, Dynamic light scattering as a powerful tool for gold nanoparticle bioconjugation and biomolecular binding studies, Analytical Chemistry 81 (2009) 9425–9432.
[49] D.A. Stuart, A.J. Haes, C.R. Yonzon, E.M. Hicks, R.P. Van Duyne, Biological applications of localised surface plasmonic phenomenae, IEE Proceedings. Nanobiotechnology 152 (2005) 13–32.
[50] I. Delfino, K. Sato, M.D. Harrison, L. Andolfi, A.R. Bizzarri, C. Dennison, S. Cannistraro, Optical spectroscopic investigation of the alkaline transition in umecyanin from horseradish root, Biochemistry 44 (2005) 16090–16097.
[51] I. Delfino, C. Piccolo, M. Lepore, Experimental study of short- and long-time diffusion regimes of spherical particles in carboxymethylcellulose solutions, European Polymer Journal 41 (2005) 1772–1780.
[52] M. Zimbone, L. Calcagno, G. Messina, P. Baeri, G. Compagnini, Dynamic light scattering and UV–vis spectroscopy of gold nanoparticle solution, Materials Letters 65 (2011) 2906–2909.
[53] S.W. Provencher, A constrained regularization method for inverting data represented by linear algebraic or integral equations, Computer Physics Communications 27 (1982) 213–227.
[54] P. Laven, MiePlot 4.3 Software Package, www.philiplaven.com/mieplot.htm.